Chapter 6
Electronic Structure of TiO_2 Studied by Far-Ultraviolet and Deep-Ultraviolet Spectroscopy

Ichiro Tanabe

Abstract The electronic structure and photocatalytic activities of TiO_2 and metal-nanoparticle-modified TiO_2 were investigated by far-ultraviolet and deep-ultraviolet spectroscopy and photodegradation reaction of methylene blue. First, spectra of naked anatase TiO_2 (Sect. 6.2) and metal (Au, Pd, Pt)-nanoparticle-modified TiO_2 (Sect. 6.3) were measured. The naked TiO_2 spectrum corresponded well with the previously reported reflection spectrum and theoretical calculations. Then, the deposition of metal nanoparticles substantially changed the spectral shape, which indicates changes in the electronic states of TiO_2, and the degree of spectral changes strongly depends on the work function of the modified metal. In addition, consistent changes of photocatalytic activities were also observed. Next, two crystalline types of TiO_2 (anatase and rutile) were compared (Sect. 6.4), and a larger enhancement of the photocatalytic activity of rutile TiO_2 upon Pt nanoparticle deposition was revealed. Subsequently, size effects of modified Au nanoparticle on electronic structures and photocatalytic activities of TiO_2 were discussed (Sect. 6.5), and it was made clear that the smaller Au nanoparticle induced the larger electronic-state changes and the higher photocatalytic-activity enhancements. These results demonstrated that the novel far-ultraviolet and deep-ultraviolet spectroscopy is a considerable promising method to investigate the electronic states of materials, leading to the development of high-efficiency optical materials such as photocatalysts and solar cells.

Keywords Titanium dioxide • TiO_2 • Metal nanoparticle • Photocatalyst • Photocatalytic activity

I. Tanabe (✉)
Department of Chemistry, School of Science and Technology, Kwansei Gakuin University, Gakuen 2-1, Sanda, Hyogo, Japan
e-mail: dnv62544@kwansei.ac.jp

Y. Ozaki, S. Kawata (eds.), *Far- and Deep-Ultraviolet Spectroscopy*,
DOI 10.1007/978-4-431-55549-0_6

6.1 Introduction

6.1.1 *TiO_2 and Metal-Nanoparticle-Modified TiO_2 as Photo-Functional Materials*

TiO_2 is considered one of the most attractive materials in a wide range of fields [1–6] and may find application as a photocatalyst [1–3] and next-generation solar-cell material [4–6]. It shows photocatalytic activity under ultraviolet (UV, <400 nm), deep-UV (DUV, <300 nm), and far-UV (FUV, <200 nm) irradiation, as its bandgap is ~3.2–3.0 eV [7]. Under irradiation with these lights, the electrons in the valence band of TiO_2 are promoted into the conduction band, and, at the same time, corresponding holes are generated in the valence band. This photoinduced charge separation is the main cause of its photocatalytic activity; the enhanced electrons and generated holes are then consumed by reduction and oxidation reactions, respectively. Several studies have confirmed that a variety of reactions can be promoted in the presence of TiO_2 and UV light, such as alcohol dehydration [8], oxidation of organic materials [9], and reduction of nitrogen oxide [10]. TiO_2 can even promote water splitting, which produces hydrogen and oxygen [11]. Therefore, it can be applied for the purification of water and air. In addition, TiO_2 is expected to be also suitable for solar cells based on photoinduced charge separation [4–6].

However, the quantum yields of most photocatalytic reactions and incident photon-to-current conversion efficiency of naked TiO_2 are extremely low (<1 %) [12]. To address this issue, a number of studies have been proposed for enhancing the charge-separation efficiency of TiO_2 [13–15]. For example, doping TiO_2 with various transition metal cations (Fe^{3+}, Ru^{3+}, V^{4+}, etc.) [13] and anions such as F^- [14] can increase its photocatalytic activity. The modification of TiO_2 with quantum dots [6] and dye molecules [4, 5] expands its wavelength range to the visible region; quantum-dot and dye-sensitive solar cells are thus considered promising candidates as the next-generation solar cells.

Among other systems, the combination of TiO_2 with metal nanoparticles has been extensively investigated in recent decades by many research groups [1, 16–21]. Loading TiO_2 with Pt nanoparticles increases its activity for hydrogen-production reactions from water and other photocatalytic reactions [16, 17]. The deposition of other metal nanoparticles (e.g., Ag, Au, Pd, and Ir) [18] also improves the photocatalytic activity of TiO_2. These metal nanoparticles function as a photoexcited electron sink, as the electron transfer from TiO_2 to metals shifts the Fermi level of TiO_2 to negative potentials, thus enhancing the photoinduced charge-separation efficiency [20, 21].

6.1.2 *Attenuated Total Reflectance (ATR)–DUV–FUV Spectroscopy*

As mentioned above, naked TiO_2 can be activated by UV, DUV, and FUV irradiations. However, the measurement of the optical properties of TiO_2 in these regions is complicated by its very large absorption (in the 200–300-nm region, the absorbance index α is $\sim 10^6$–10^7 cm^{-1}) [22]. Irradiation in the DUV–FUV region can provide critical information about the electronic states of materials and is typically employed for research activities and a diverse range of applications [23–25]; therefore, the investigation of TiO_2 and modified TiO_2 materials in this region is very important. However, only a few studies provide systematic information about the modification of TiO_2 through spectrum observations in the DUV–FUV region. Most spectroscopic investigations in this region have been carried out only by reflectance or diffuse reflectance spectra measurements, and the measurement ranges were mostly limited to the DUV region (>200 nm) [26]. Moreover, the effects of surface modifications such as metal nanoparticle deposition on TiO_2 electric states cannot be easily estimated; thus, many studies on the enhancement of the charge-separation efficiency of TiO_2 are performed using polycrystalline TiO_2 powders and films [18–21]. Therefore, a versatile DUV–FUV measurement method that can be applied not only to single crystals but also to polycrystalline forms is needed.

We have recently developed a completely new DUV–FUV spectrometer based on ATR [23–25] that enables the measurement of the spectra of liquid and solid samples such as water [27], aqueous solutions [28, 29], and organic molecules [30–32] in the 140–300-nm region. During the ATR–DUV–FUV measurement, samples are typically placed on a sapphire internal reflection element (IRE), and ATR spectra are measured using the evanescent wave as a probe light [27]. This method allowed us for the first time to successfully observe the entire first electronic-transition absorption band of water and aqueous solutions without band saturation [27–29]. Moreover, a comparison of the observed spectra of organic molecules such as alkanes [32], alcohols [30], and ketones [31] with the corresponding quantum chemical calculations revealed the existence of Rydberg transitions in the liquid states. The more detailed description of the instrument is described in Chap. 2 *Instrumentation for FUV spectroscopy*.

6.2 Electronic States of Anatase TiO_2 Studied by DUV–FUV Spectroscopy [33]

Figure 6.1a shows a typical DUV–FUV spectrum in the 150–300-nm region of a commercial anatase TiO_2 particle (diameter = $\sim$5 μm, ST-41, Ishihara Sangyo Kaisha, Ltd.). As the refraction index at 250 nm of anatase TiO_2 ($\sim$2.5) is higher than that of sapphire ($\sim$1.8), ATR does not occur at their interface. However, the contact area between TiO_2 and the sapphire IRE is very small (point contact, ide-

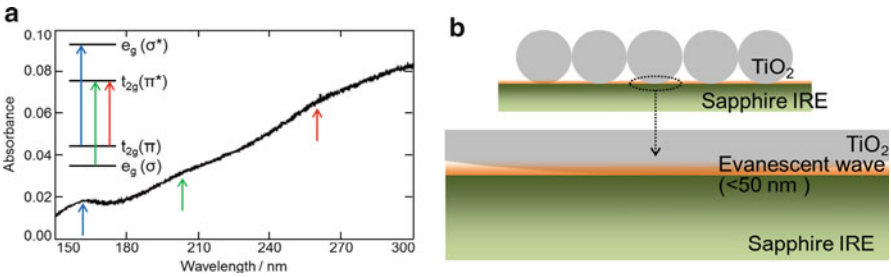

Fig. 6.1 (**a**) A typical DUV–FUV spectrum of TiO_2 and (**b**) the ATR-spectrometer measurement scheme

ally), because a spherical TiO_2 particle was used. Therefore, the absorption spectra of TiO_2 in the evanescent wave range were successfully measured (Fig. 6.1b). In this case, the penetration depth of the evanescent wave is less than 50 nm, with an incident angle of 70° and a measured wavelength region of 150–300 nm in air ($n = 1$).

In a previous study of Hosaka and coworkers [34], the reflection spectra of anatase TiO_2 single crystals were measured in the 40–620-nm wavelength range using synchrotron orbital radiation. According to these studies, the measured reflection spectra of anatase TiO_2 have three peaks in the 150–300-nm region (at ~155, 200, and 260 nm), in agreement with the absorption spectrum discussed here. The measured spectra were interpreted based on electronic-structure calculations performed by these authors [34, 35] and other research groups [36]. Hosaka and coworkers calculated the electric states of anatase TiO_2 using the linear combination of atomic orbital (LCAO) approximation with a discrete variational (DV)-Xα method based on the TiO_6 cluster model. By comparing the experimental and calculated spectra, they assigned the spectra in the 120–400-nm range to the transition from O(2p) to Ti(3d) states.

In addition, Sério and coworkers [37] measured the DUV–FUV absorption spectra of TiO_2 using a synchrotron-radiation facility; however, as they reported, only the data obtained in the DUV region (>200 nm) were considered to be reliable because of a strong influence of the adsorbed water. In line with their results, in our study we observed very weak and broad absorption bands at ~200 and 260 nm (Fig. 6.1a). Sério and coworkers assigned these two bands to the $e_g(\sigma) \rightarrow t_{2g}(\pi^*)$ and $t_{2g}(\pi) \rightarrow t_{2g}(\pi^*)$ transitions, respectively, based on a molecular orbital energy-level diagram [19] and band structures [19, 36] calculated by other groups. The comparison of the present DUV–FUV spectrum with these calculations suggests that the clear peak at 160 nm may be assigned to the $t_{2g}(\pi) \rightarrow e_g(\sigma^*)$ transition (inset in Fig. 6.1a). It should be noted that the upper $t_{2g}(\pi^*)$ and $e_g(\sigma^*)$ and lower $t_{2g}(\pi)$ and $e_g(\sigma)$ orbitals mainly consist of Ti(3d) and O(2p) orbitals, respectively.

The present spectral shape in the 150–180-nm region clearly differs from that of water, and thus the measurement of the absorption spectrum of TiO_2 in the 150–300-nm region, including the FUV region, was successfully achieved. The

assignments of the three bands to these electric states were confirmed by the reported theoretical calculations. Notably, this DUV–FUV spectrum was obtained using a 30-W deuterium lamp and commercial TiO_2 powder, instead of synchrotron orbital radiation and a TiO_2 single crystal.

6.3 Consistent Changes in the Electronic States and Photocatalytic Activities of TiO_2 upon Metal (Au, Pd, Pt)-Nanoparticle Deposition [33]

6.3.1 TiO_2 Spectral Changes upon Metal-Nanoparticle Deposition

TiO_2 and metal (Pt, Pd, Au) colloids were mixed in an agate mortar until the solvent completely evaporated. The DUV–FUV spectra of TiO_2 with Pt nanoparticles (diameter = 1–6 nm) were then measured. Figure 6.2 compares the DUV–FUV spectra of the TiO_2–Pt nanoparticles with that of TiO_2. When the amount of the mixed Pt nanoparticle is 0.04 wt% (green line in Fig. 6.2), the absorption intensity at longer wavelengths decreases, while that at shorter wavelengths increases upon Pt-nanoparticle deposition. The amount of the mixed Pt nanoparticle was changed from 0.02 to 0.12 wt%. The DUV–FUV spectrum of TiO_2 mixed with the 0.04 wt% Pt nanoparticle showed the largest increase in the shorter-wavelength region; when the amount of the Pt-nanoparticle was larger than 0.06 wt%, the absorption intensity was suppressed in the entire wavelength range. This indicates that the increase in the shorter-wavelength region is not due to the absorption of Pt nanoparticles.

If TiO_2 comes in contact with a metal with a higher work function, the electrons in TiO_2 flow into the metal until the Fermi levels become equal [1]. In this study, we

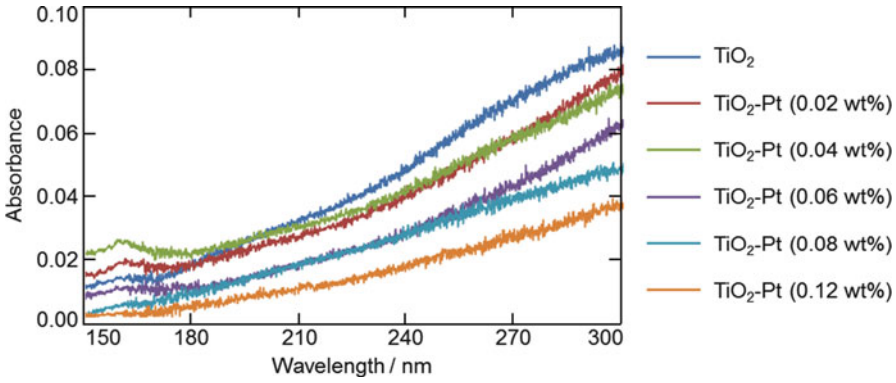

Fig. 6.2 DUV–FUV spectral changes of TiO_2 with various concentrations (0.00–0.12 wt%) of Pt nanoparticles

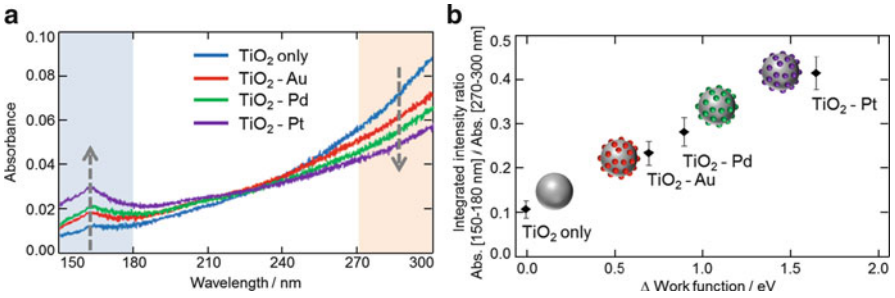

Fig. 6.3 (**a**) DUV–FUV spectra of TiO_2 (*blue*) and Au (*red*)-, Pd (*green*)-, and Pt (*purple*)-modified TiO_2. (**b**) Integrated intensity ratio between the absorption in the 150–180-nm region and that in the 270–300-nm region vs. the work-function difference between TiO_2 and each metal

determined the work functions of TiO_2 and Pt to be ~4.0 and 5.7 eV, respectively; thus, the electrons transfer from TiO_2 to Pt. As a result, the number of electrons in the relatively high-energy levels (i.e., electrons that can be excited at a relatively longer wavelength) is decreased, leading to a suppression of the absorption intensity at longer wavelengths. However, a Pt nanoparticle on TiO_2 can act as a sink for the photoexcited electrons [20, 21], which can enhance the charge-separation efficiency as described in Sect. 6.1.1. This results in an increase in the absorption intensity at shorter wavelengths. This enhancement may also occur at longer wavelengths; however, in this case, the total change of the absorption intensity is affected by both the enhancement and the decrease in the electrons upon contact of TiO_2 with Pt.

In addition, we also used Pd and Au instead of Pt nanoparticles on TiO_2 and measured the DUV–FUV spectra of the resulting systems (Fig. 6.3a). In all the studied cases, the absorption intensity at longer wavelengths decreases, while that at shorter wavelengths increases. The absorption intensity over the entire wavelength region changes by several percentage points depending on the sample, because the TiO_2 particle is not a perfect sphere; as a result, the amount of TiO_2 in the evanescent wave changes, but the spectral shapes of each sample are virtually the same. In order to provide an in-depth description of the degree of the spectral changes, we calculated an integrated intensity ratio between the absorption in the 150–180-nm region and that in the 270–300-nm region.

The integrated intensity ratios of TiO_2, TiO_2–Au, TiO_2–Pd, and TiO_2–Pt were determined to be 0.133 ± 0.018, 0.252 ± 0.025, 0.295 ± 0.030, and 0.423 ± 0.035 nm (average $\pm$ standard deviation, $n = 15$), respectively. Figure 6.3b displays the plots of the obtained ratios as a function of the difference in the work function between TiO_2 (~4.0 eV) and each metal (Au, Pd, Pt ~4.7, 4.9, 5.7 eV, respectively). Notably, a strong positive correlation between the intensity ratio and the work-function difference was found, indicating that a larger work-function difference results in a larger number of electrons that flow from TiO_2 into the metal as well as stronger enhancement of the charge separation.

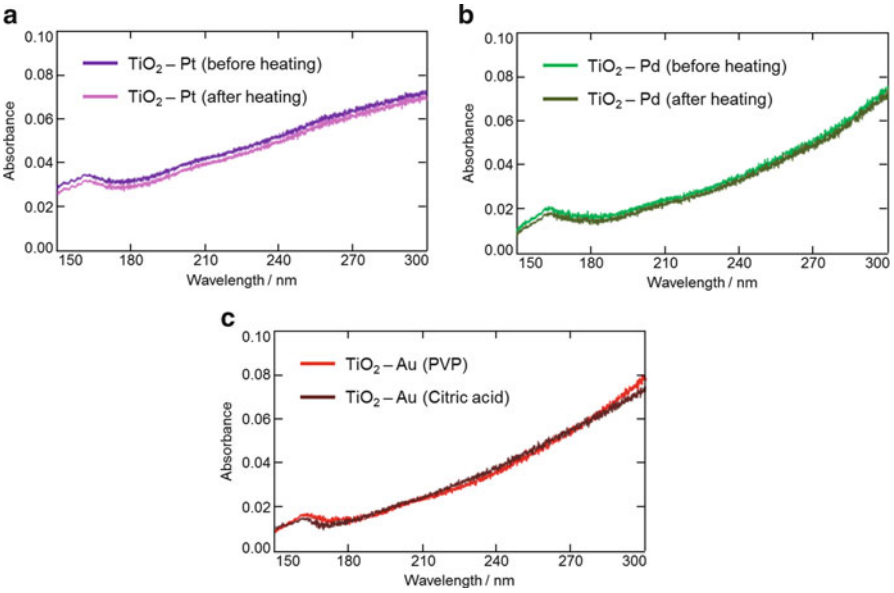

Fig. 6.4 (**a**) DUV–FUV spectra of TiO_2–Pt nanoparticles before (*purple*) and after (*pink*) heating (at 200 °C for 1 h, to remove the protecting agent PVP). (**b**) ATR–FUV spectra of TiO_2–Pd nanoparticles before (*green*) and after (*deep green*) heating (200 °C, 1 h). (**c**) ATR–FUV spectra of TiO_2–Au protected by PVP (*red*) and citric acid (*brown*) nanoparticles

To confirm the effect of the protecting agent (PVP) of the metal nanoparticles, it was removed by heating TiO_2–Pt (Fig. 6.4a) and TiO_2–Pd (Fig. 6.4b) at 200 °C for 1 h [38]. The DUV–FUV spectra did not change; in addition, a comparison of the DUV–FUV spectra of TiO_2–Au protected by PVP and citric acid (Fig. 6.4c) hardly differed. These results clearly suggest that the protecting agents have no substantial effects on the DUV–FUV spectra.

6.3.2 *Photocatalytic-Activity Enhancement of TiO_2 upon Metal-Nanoparticle Deposition*

The photocatalytic activities of TiO_2 and TiO_2 modified with Au, Pt, and Ad nanoparticles were estimated by the photodegradation reaction of methylene blue. Methylene blue was purchased from Wako Pure Chemical Industries, Ltd. A Hg–Xe lamp (Luminar Ace LA-300UV, Hayashi Watch Works) equipped with a UV-pass filter (wavelength = 300–350 nm, UTVAF-50S-34U, CVI Laser, LLC.) was used as the UV-light source. Methylene blue aqueous solution (10 μM, 10 mL) was mixed with TiO_2, TiO_2–Au, TiO_2–Pd, and TiO_2–Pt powder (5 mg) using a magnetic stirrer, followed by UV irradiation (∼10 μW cm^{-2}) for 60 min. After the irradiation, TiO_2

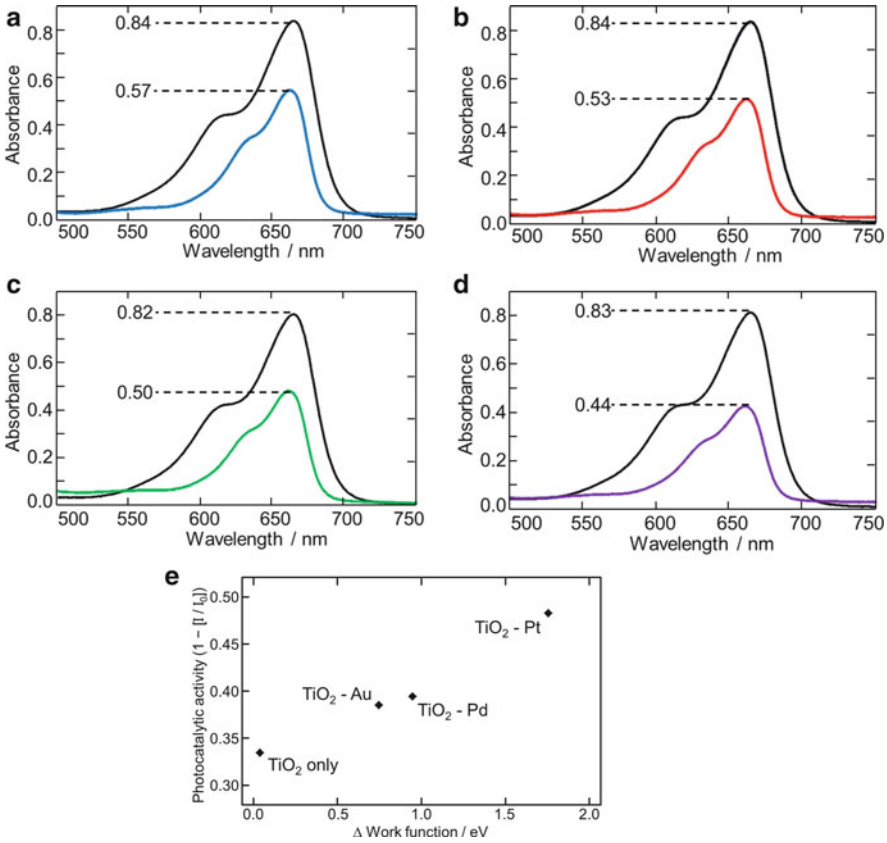

Fig. 6.5 (**a**–**d**) Absorption spectra of methylene blue aqueous solution before (*black*) and after (*color*) UV irradiation with (**a**) TiO_2 and (**b**) Au-, (**c**) Pd-, and (**d**) Pt-modified TiO_2. *Inset* values represent the absorption at 665 nm. (**e**) Photocatalytic activity ($1 - [I/I_0]$) plotted against the work-function difference between TiO_2 and each metal

was separated from the solution by centrifugation (15,000 rpm, 1 min). Before and after the UV irradiation, absorption spectra of the methylene blue aqueous solution were measured; the results are shown in Fig. 6.5a–d. The photocatalytic activity of each sample was estimated using Eq. (6.1), where I_0 and I represent the absorption intensities at 665 nm before and after the photodegradation reaction, respectively:

$$\text{Photocatalytic activity} = 1 - I/I_0 \tag{6.1}$$

Figure 6.5e shows the relationship between the photocatalytic activity and work-function difference between TiO_2 and each metal. Notably, a strong positive correlation, similar to that of the degree of spectral changes shown in Fig. 6.3b, was found.

This strong positive correlation indicates that the larger work-function difference results in an increased electron inflow from TiO_2 to the metal and, therefore, in a stronger enhancement of the charge separation, thereby increasing the TiO_2 photocatalytic activity (Fig. 6.5). This finding is in agreement with previous studies [18, 39] that reported a clear correlation between the work function of the metals and the photocatalytic activity assessed in other reactions such as the generation of NH_3 from N_3^- [18] and H_2 from the dehydration of 2-propanol [39]. These results indicate that the photocatalytic activity of modified TiO_2 can be systematically estimated by simple spectral measurements.

6.4 Significant Enhancement of the Photocatalytic Activity of Rutile TiO_2 Compared to That of Anatase TiO_2 upon Pt-Nanoparticle Deposition [40]

6.4.1 Two Types of Crystalline TiO_2: Anatase and Rutile

The two types of readily available varieties of crystalline TiO_2, anatase and rutile (Fig. 6.6), exhibit different chemical, physical, optical, and photocatalytic properties [19, 26, 41]. The bandgap energy of anatase TiO_2 (~3.2 eV) is higher than that of rutile TiO_2 (~3.0 eV) [19]; the reflectance spectra of anatase and rutile TiO_2 in the DUV region have also been reported [26]. However, until quite recently, several difficulties have limited the measurement of the optical properties of TiO_2 in the FUV region; thus, it has not been possible to clarify the differences in the optical properties of anatase and rutile TiO_2 in the FUV region, despite the fact that this

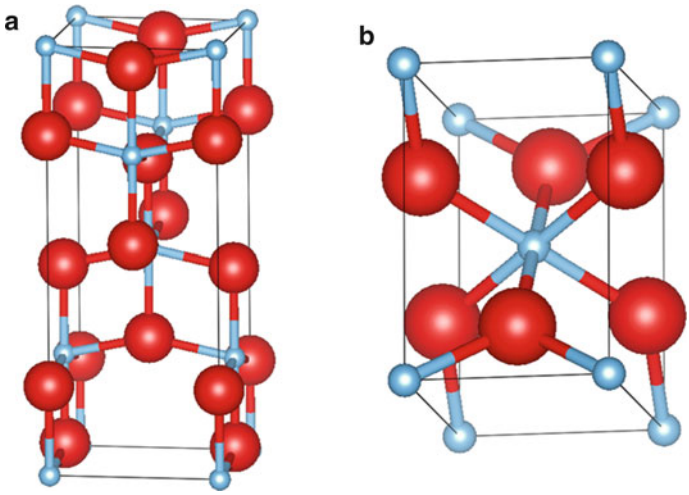

Fig. 6.6 Schematic representation of (**a**) anatase and (**b**) rutile structures

region potentially provides substantial information about the electronic states of these materials. TiO_2 is activated upon UV irradiation (<390 nm and <410 nm for the anatase and rutile phases, respectively); therefore, the investigation of the optical properties in both the DUV and FUV regions is important.

In addition, the differences in the electronic state and photocatalytic activity between anatase and rutile TiO_2 upon surface modifications such as metal-nanoparticle deposition are not well understood. A simple and systematic method to measure these differences for material design is thus needed. Herein, we measured the DUV–FUV spectra of anatase and rutile TiO_2 particles with a 5-μm secondary particle diameter and 200- and 40-nm diameters, respectively. Subsequently, the DUV–FUV spectra of TiO_2 with Pt nanoparticles were also obtained, and the spectral changes and photocatalytic activities of all TiO_2 species were investigated.

6.4.2 DUV–FUV Spectra of Various Sizes Anatase and Rutile TiO_2

The DUV–FUV spectra in the 150–300-nm wavelength region of commercial anatase and rutile TiO_2 particles with a 5-μm secondary particle diameter and 200- and 40-nm diameter, respectively, were measured. The spectra of the anatase TiO_2 particles showed a broad band at ∼160 nm, regardless of the particle size, which, as mentioned in Sect. 6.2, is assigned to the $t_{2g}(\pi) \rightarrow e_g(\sigma^*)$ transition (Fig. 6.7a). In addition, the spectral intensities of rutile TiO_2 particles were found to be lower than those of anatase TiO_2 (Fig. 6.7b), and the spectra showed no clear peak in the FUV region. Figure 6.8a–h displays the SEM images of the TiO_2 particles. Commercial TiO_2 nanoparticles have definite diameters for both the anatase and rutile phases (200 and 40 nm, respectively); however, for TiO_2 particles with 5-μm secondary particle diameters, the original particle diameters of the anatase and rutile phases vary by several dozen and several hundred nanometers, respectively. Absorbance of the DUV–FUV spectrum of anatase TiO_2 with a 5-μm secondary particle diameter is similar to that of anatase TiO_2 with a 40-nm particle diameter (Fig. 6.7a). Likewise, the intensity of rutile TiO_2 with a 5-μm secondary particle diameter is similar to that of rutile TiO_2 with a 200-nm particle diameter (Fig. 6.7b). These results suggest that the intensity of the TiO_2 spectra is largely dependent on the particle size. This is because the amount of TiO_2 with 40-nm-diameter particles in the evanescent wave range (Fig. 6.8i) is larger than that of TiO_2 with 200-nm-diameter particles (Fig. 6.8j).

6.4.3 DUV–FUV Spectral Changes of Anatase and Rutile TiO_2 upon Pt-Nanoparticle Deposition

The DUV–FUV spectra of TiO_2 modified with Pt nanoparticles were also measured. The Pt nanoparticles (1–6 nm in diameter) were deposited by mixing TiO_2 particles

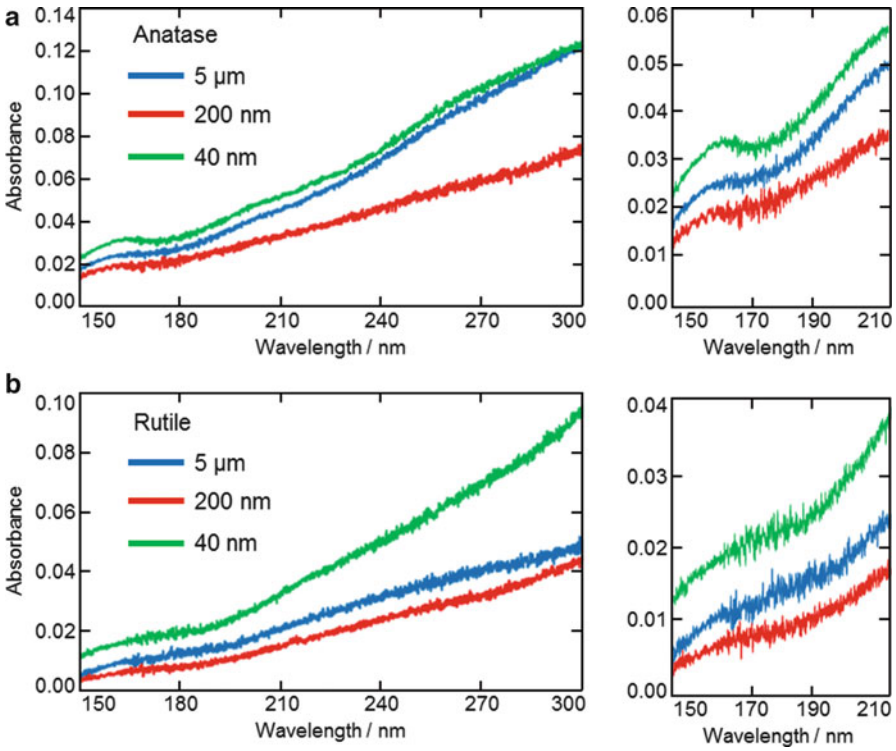

Fig. 6.7 DUV–FUV spectra of (**a**) anatase and (**b**) rutile TiO_2 particles with diameters of (*blue*) 5 μm, (*red*) 200 nm, and (*green*) 40 nm

(1 g) with commercially available Pt nanoparticle colloids (200 μL, 10 mM in water/ethanol solution, protected by PVP, Wako Pure Chemical Industrial, Ltd.) in an agate mortar until the solvent completely evaporated. Figure 6.9a–f compares the ATR–FUV spectra of TiO_2–Pt nanoparticles (red lines) with those of TiO_2 (black lines). The ATR–FUV spectra of rutile TiO_2 particles modified with Pt nanoparticles and those of anatase TiO_2 particles show bands at ∼170 nm and ∼160 nm, respectively. This behavior results from the differences in the electronic structures of the anatase and rutile phases, as shown by previous calculations [42]. The spectral differences between the anatase and rutile phases in the DUV (>200 nm) region have been previously reported [26]; according to this study, the band wavelengths of rutile-phase TiO_2 are longer than those of anatase-phase TiO_2. By employing an ATR–FUV spectrometer, we can compare for the first time the optical spectra of anatase and rutile TiO_2 in the FUV region.

Upon Pt-nanoparticle deposition, the spectral intensity of the anatase-TiO_2 particles (Fig. 6.3a–c) at longer wavelengths decreases, while that at shorter wavelengths increases. As described in Sect. 6.3, the decrease in the intensity in the longer-wavelength region is due to a charge transfer at the TiO_2–Pt interface,

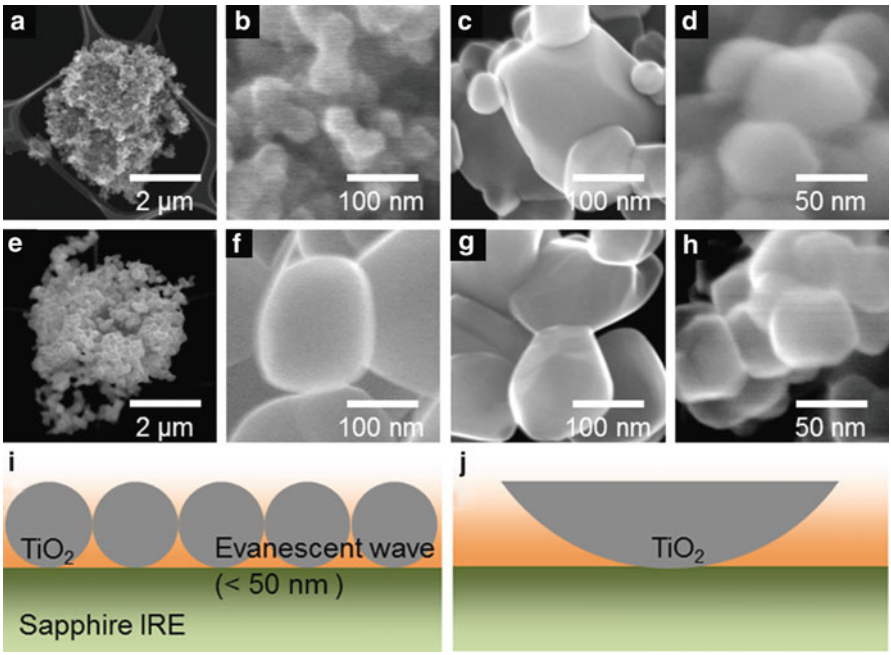

Fig. 6.8 SEM images of (**a**–**d**) anatase and (**e**–**h**) rutile TiO_2 particles with diameters of (**a**, **b**, **e**, and **f**) 5 μm, (**c** and **g**) 200 nm, and (**d** and **h**) 40 nm. (**i** and **j**) Scheme of ATR–FUV spectrometer measurement of TiO_2 particles with diameters of (**i**) 40 nm and (**j**) 5 μm

and the increase in the shorter-wavelength region is due to the enhancement of the charge-separation efficiency upon the deposition of the Pt nanoparticles. The work function of TiO_2 (∼4.0 eV for anatase-phase TiO_2) is smaller than that of Pt (∼5.7 eV). Therefore, when TiO_2 contacts the Pt nanoparticles, the electrons in TiO_2 flow into the Pt nanoparticles until the Fermi levels are equalized. As a result, the number of electrons in the relatively high-energy levels (i.e., electrons that can be excited at a relatively longer wavelength) is decreased, resulting in the suppression of the spectral intensity in the longer-wavelength region. In contrast, Pt nanoparticles on TiO_2 can act as a sink for the photoexcited electrons, resulting in an enhancement of the charge-separation efficiency and an increase in the spectral intensity in the shorter-wavelength region. This process may also occur in the longer-wavelength region; however, the total change in the spectral intensity depends on this enhancement and the decrease in the number of electrons upon contact between TiO_2 and Pt nanoparticles.

In contrast, the spectral intensity of the rutile-TiO_2 nanoparticles (Fig. 6.9d–f) increases over the entire region upon deposition of Pt nanoparticles. When anatase TiO_2 is modified with Au nanoparticles, the intensity in the longer-wavelength region decreases, as it does for the anatase TiO_2–Pt nanoparticles based on

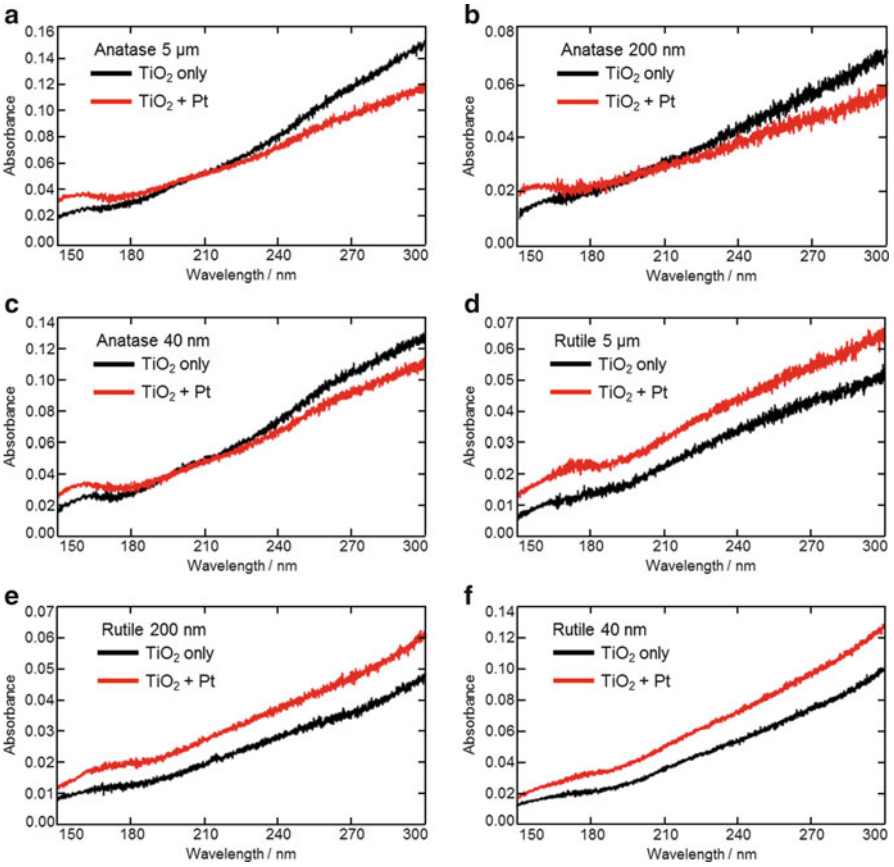

Fig. 6.9 DUV–FUV spectra of (**a**–**c**) anatase and (**d**–**f**) rutile TiO_2 particles with diameters of (**a** and **d**) 5 μm, (**b** and **e**) 200 nm, and (**c** and **f**) 40 nm, before (*black*) and after (*red*) the deposition of Pt nanoparticles

the electron transfer described above. The work function of Au (∼4.7 eV) is approximately 1.0 eV lower than that of Pt, while that of rutile TiO_2 is 0.2 eV lower than that of anatase TiO_2 (at most) [19, 41]. Therefore, if the magnitude of the effect of the charge-separation enhancement for rutile TiO_2 is the same as that for anatase TiO_2, the intensity in the longer-wavelength region should decrease. However, in practice, the spectral intensity of rutile TiO_2 increases even in the longer-wavelength region. In this regard, the increase in the spectral intensity implies an enhancement of charge separation, as ascribed in Sect. 6.3.1. Therefore, these results indicate that the magnitude of the effect of charge-separation enhancement for rutile TiO_2 is higher than that for anatase TiO_2. In order to estimate this enhancement, we investigated their photocatalytic activities.

6.4.4 Photocatalytic-Activity Enhancement in Anatase and Rutile TiO_2 upon Pt-Nanoparticle Deposition

The photocatalytic activities of TiO_2 particles with and without Pt nanoparticles were estimated based on the photodegradation reaction of methylene blue. A methylene blue aqueous solution (20 μM, 20 mL), including TiO_2 particles with/without Pt nanoparticles (5 mg), was irradiated with UV light (300–350 nm, ~10 μW cm^{-2}) for 30 min, and the absorption spectra before and after UV irradiation were measured (Fig. 6.10). The photocatalytic activity of each sample was also estimated using Eq. (6.1).

Figure 6.11(a) (anatase TiO_2) and (b) (rutile TiO_2) show the plots of the photocatalytic activities of TiO_2 (black) and TiO_2 with Pt nanoparticles (red) as a function of the particle diameter. For a 5-μm secondary particle diameter and 200-nm-diameter TiO_2 particles, the photocatalytic activity of anatase TiO_2 is higher than that of rutile TiO_2 of the same size, in agreement with previous studies [3]. For rutile TiO_2, a smaller TiO_2 particle shows a larger photocatalytic activity, and TiO_2 with a 5-μm secondary diameter shows the smallest photocatalytic activity. These trends are a result of the smaller particle size and the consequent larger surface area [43].

The anatase TiO_2 particles with 40-nm diameters show an exceptionally low photocatalytic activity, probably because of the synthesis of small anatase TiO_2 nanoparticles, which requires a lower temperature than that of large anatase particles and rutile particles [44]. In addition, anatase TiO_2 particles with 40-nm diameters are characterized by a larger number of lattice defects, which may decrease the photocatalytic activity [45]. The photocatalytic activities of all TiO_2 nanoparticles are enhanced upon deposition of Pt nanoparticles. The photocatalytic activities of anatase TiO_2 were determined to be 0.47, 0.53, and 0.33 (5-μm-, 200-nm-, and 40-nm-diameter particles, respectively) and increased to 0.52, 0.62, and 0.36, respectively, upon the deposition of Pt nanoparticles. The photocatalytic activities of rutile TiO_2 were found to be 0.13, 0.23, and 0.44 (5-μm-, 200-nm-, and 40-nm-diameter particles, respectively) and increased to 0.18, 0.28, and 0.55, respectively. The "enhancement factor" was calculated for each TiO_2 particle as the ratio between the photocatalytic activity of TiO_2 modified with the Pt nanoparticles and that of TiO_2 alone [46, 47]. As shown in Fig. 6.11c, the rutile TiO_2 particles (open circles) show a higher photocatalytic-activity enhancement than the anatase TiO_2 particles (filled circles). Several research groups have reported that the photocatalytic activity of TiO_2 is improved upon the deposition of metal nanoparticles [1, 16–21, 48]. However, most of these groups have focused on either anatase TiO_2 or a mixture of anatase and rutile TiO_2 [16–21], because both these systems show a higher photocatalytic activity in many reactions than bare rutile TiO_2. Rutile TiO_2 has been primarily used for the investigations of reaction mechanisms. For example, Li and coworkers showed that the (110) surface of rutile TiO_2 can be more selectively deposited with Pt nanoparticles than the (001) surface and that the photocatalytic activity is improved by Pt deposition [48]. However, no studies are available about a

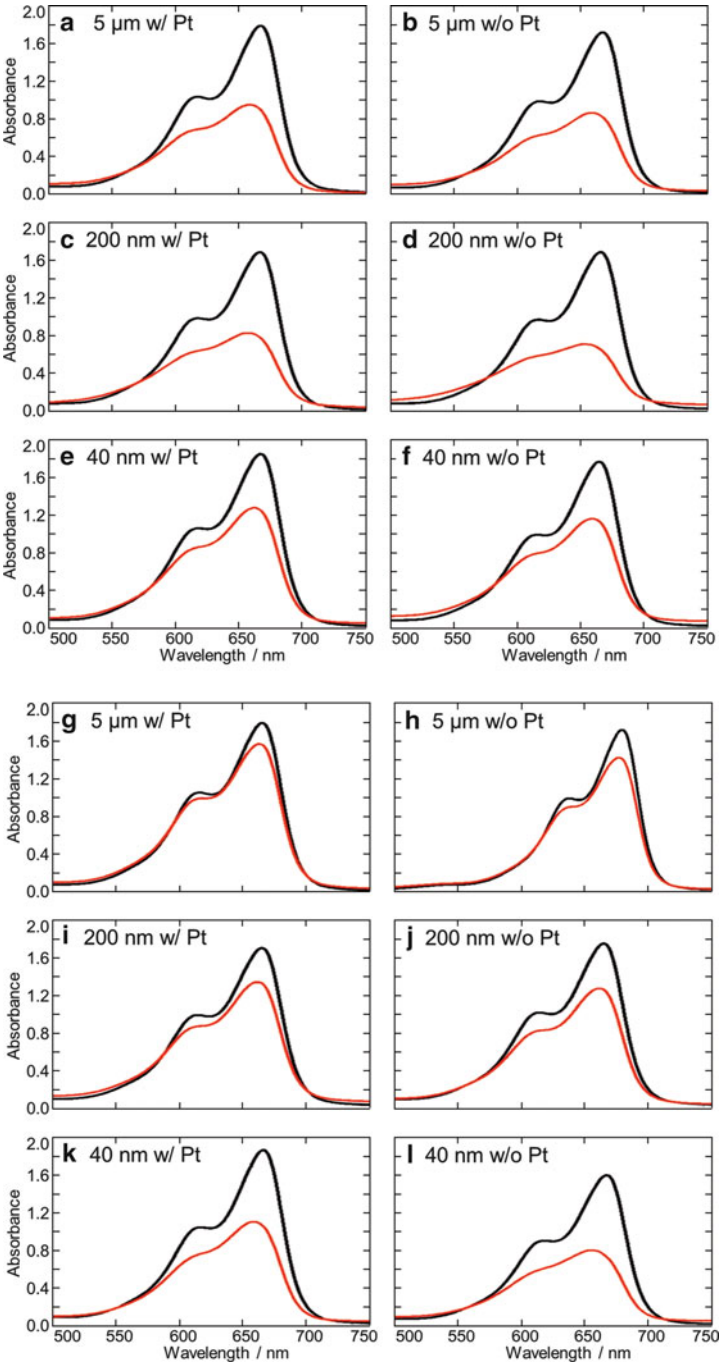

Fig. 6.10 Absorption spectra of aqueous methylene blue before (*black*) and after (*color*) UV irradiation with (**a**–**f**) anatase or (**g**–**l**) rutile TiO_2. TiO_2 particle size and state (i.e., with/without Pt nanoparticles) are displayed in each graph

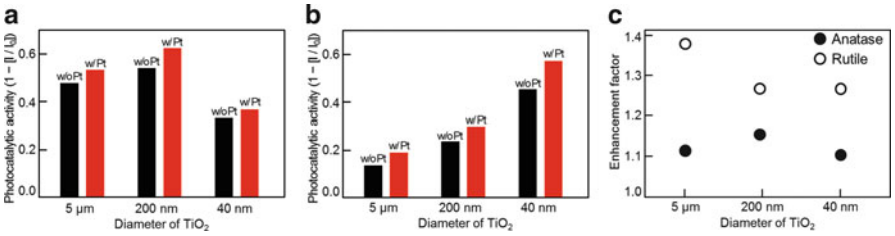

Fig. 6.11 Photocatalytic activities ($1 - [I/I_0]$) of (**a**) anatase and (**b**) rutile TiO_2 particles (*black*) before and (*red*) after the deposition of Pt nanoparticles. (**c**) Enhancement factors of (*filled circle*) anatase and (*open circle*) rutile TiO_2 particles. TiO_2 particle diameters are 5 μm, 200 nm, and 40 nm

systematic comparison of anatase and rutile TiO_2 in terms of their optical and/or photocatalytic property changes upon metal deposition. In our study, we have systematically compared the electronic-state changes and photocatalytic activity of anatase and rutile TiO_2; based on the DUV–FUV spectral measurements and estimations of the photodegradation reaction activity, we have shown that the enhancement of the charge-separation efficiency upon Pt-nanoparticle deposition is higher for rutile TiO_2 than for anatase TiO_2.

6.5 Size Effect of Modified Au Nanoparticles on TiO_2 Electronic States [49]

6.5.1 Size Effect of Modified Au Nanoparticles on the TiO_2 Photocatalytic Activity Under UV- and Visible-Light Irradiation

The effects of the Au-nanoparticle size on the photocatalytic activity of TiO_2–Au nanoparticles have been reported. For instance, Idriss and coworkers estimated the photocatalytic activity of TiO_2 modified with Au nanoparticles, whose size ranged between 3 and 30 nm, based on the photocatalytic hydrogen production from ethanol under UV-light irradiation [50]. When they adopted anatase TiO_2, the photocatalytic-reaction rate was not affected by the Au-nanoparticle size over the 3–12-nm range. When the size was increased to 16 nm, the reaction rate of the anatase TiO_2–Au nanoparticle was considerably reduced. In the case of rutile TiO_2 with Au nanoparticles with a diameter of 20–35 nm, the photocatalytic activity was found to be virtually independent of the Au-nanoparticle size.

Tatsuma's group has reported that the responsible wavelength range of TiO_2 can be expanded into the visible region by decorating TiO_2 with Au nanoparticles that absorb visible light via the localized surface plasmon resonance (LSPR) [51–53]. They used the deposited Au nanoparticles with different sizes (e.g., 15, 40,

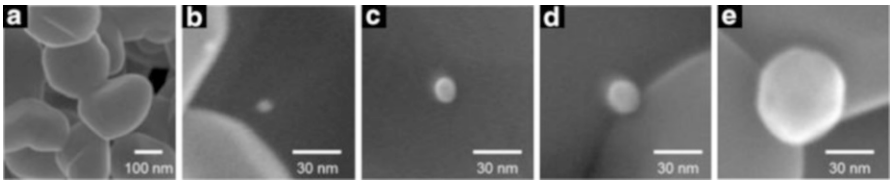

Fig. 6.12 SEM images of (**a**) TiO_2 and Au-modified TiO_2 with Au-nanoparticle diameters of (**b**) 5 nm, (**c**) 10 nm, (**d**) 20 nm, and (**e**) 60 nm

and 100 nm) and found that the quantum efficiency proportionally increased with the particle size, while the maximum photocurrent decreased under visible-light irradiation [53]. Ohtani et al. [54] measured the visible-light-induced photocatalytic-reaction rate of the oxidation reaction of 2-propanol. In their study, the Au-particle size on TiO_2 was varied in the 10–60-nm range, and a positive relationship was found between the particle size and the photocatalytic activity under visible-light irradiation.

Heretofore, only a few studies about the electronic-state changes of TiO_2–Au nanoparticle as a function of the Au-nanoparticle size have been reported. Kamat and coworkers measured the Fermi levels of TiO_2–Au nanoparticle samples (the diameters of the Au nanoparticles were 3, 5, and 8 nm on average) under UV-light irradiation [55]. However, the particle-size range was strictly limited to 3–8 nm, and no information about the shape of the Au nanoparticles was provided. The photocatalytic activity is strongly related to its electronic states, and, therefore, insight into the electronic states may help understand the mechanism of the photocatalytic enhancement and develop high-efficiency optical materials such as solar cells.

6.5.2 Size Effect of Modified Au Nanoparticles on TiO_2 Electronic States

Spherical Au colloids (diameters of 5, 10, 20, and 60 nm, aqueous solution, protected by hexadecyltrimethylammonium bromide, CTAB) were purchased from Tanaka Kikinzoku Kogyo. Anatase or rutile TiO_2 powder (5-μm secondary particle diameter) and Au colloids were mixed in an agate mortar until the solvent completely evaporated. In this study, the amount of colloids was regulated to obtain a similar number of Au nanoparticles ($\sim 3.8 \times 10^{10}$ per 1 g TiO_2). Figure 6.12 shows the typical SEM images of Au nanoparticles on rutile TiO_2 (5-μm secondary particle diameter; the original particle diameter is several hundred nanometers).

Then, the DUV–FUV spectra of the TiO_2–Au nanoparticles were measured. Upon the deposition of Au nanoparticles on anatase TiO_2, the spectral intensity at longer wavelengths (> about 210 nm) decreased, while that at shorter wavelengths (< about 210 nm) increased independently from the size of Au (Fig. 6.13a); these

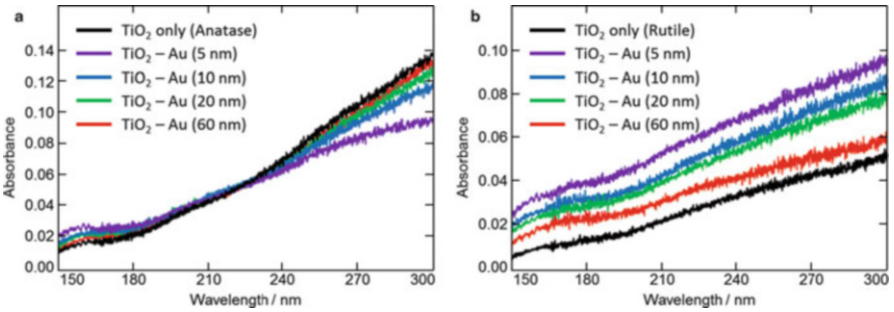

Fig. 6.13 DUV–FUV spectra of (**a**) anatase and (**b**) rutile TiO_2 with/without Au nanoparticles (5, 10, 20, and 60 nm)

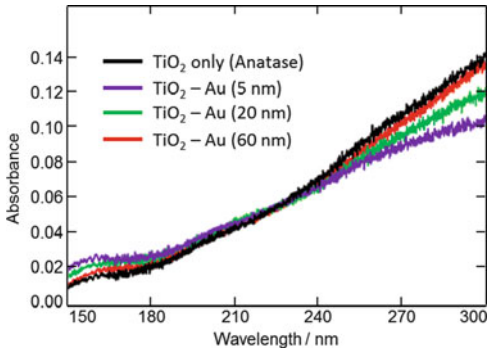

Fig. 6.14 DUV–FUV spectra of anatase TiO_2 with/without Au nanospheres (5, 20, and 60 nm). The weight of the Au nanospheres is regulated to be approximately the same

spectral changes are a result of the electron transfer from TiO_2 to the metal and the enhancement of the charge separation, respectively, as discussed in Sect. 6.3.1. In addition, the degree of the spectral changes at both longer and shorter wavelengths increased as the size of the deposited Au nanoparticles decreased. When rutile TiO_2 was used (Fig. 6.13b), the spectral intensity after the deposition of the Au nanoparticles increased over the entire wavelength region, similarly to the effect of the deposition of the Pt nanoparticles (Fig. 6.9d–f). The degree of the spectral changes also increased as the size of the deposited Au nanoparticles decreased.

Even with a similar weight of the deposited Au nanoparticles ($\sim 1.3 \times 10^{-4}$ g on 1 g TiO_2), the amount of spectral changes decreased as the size of the Au nanoparticles increased (Fig. 6.14).

These results suggest that smaller Au nanoparticles lead to larger electronic-state changes, which in turn may exert a strong effect on the photocatalytic activities. Therefore, these were measured based on the photodegradation reaction of methylene blue. The experimental details are described in the Sects. 6.3.2 and 6.4.4.

The photocatalytic activities of TiO_2 alone and TiO_2 with Au nanospheres of size 5, 10, 20, and 60 nm were determined to be 0.30 ± 0.030, 0.51 ± 0.031, 0.41 ± 0.024, 0.37 ± 0.043, and 0.33 ± 0.058, respectively (average $\pm$ standard

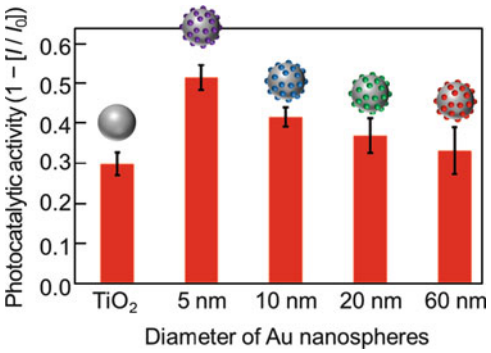

Fig. 6.15 Photocatalytic activities ($1 - [I/I_0]$) of anatase TiO_2 with/without Au nanospheres of various sizes

deviation, $n = 3$). As shown in Fig. 6.15, the photocatalytic activity strongly depends on the Au size, i.e., TiO_2 with smaller Au nanoparticles shows a higher photocatalytic activity. Our results are in agreement with those of Wei and coworkers, who reported that the photocatalytic activity of TiO_2 with ~5-nm Au is larger than that of TiO_2 with ~40-nm Au under UV-light irradiation [56]. From the results obtained from the DUV–FUV spectra (Figs. 6.13 and 6.14) and photocatalytic activities (Fig. 6.15), we concluded that the electronic state changed significantly and the photocatalytic activities increased as the Au size decreased, confirming that these strongly depend on the Au-nanoparticle size.

We then measured the DUV–FUV spectra of TiO_2–Au nanorod samples with various aspect ratios. All Au nanorods have the same diameter (25 nm), and their lengths are 34, 47, and 60 nm, with the corresponding aspect ratios being 1.36, 1.88, and 2.40, respectively. The SEM images of the Au nanorods are shown in Fig. 6.16. Au nanorods (purchased from Sigma-Aldrich Co. LLC.) were dissolved in the aqueous solution with CTAB used as a stabilizer. The number of Au nanorods was chosen to be $\sim 3.8 \times 10^{10}$ per 1 g TiO_2 (as for the Au nanospheres). As shown in Fig. 6.17, no significant changes in the DUV–FUV spectra of TiO_2 modified with these three types of Au nanorods were observed. This result suggests that the electronic state of TiO_2 may mainly depend on the diameter of the modified Au nanoparticles, with the length (i.e., aspect ratio) of the nanorods exerting only a small effect.

In addition, we synthesized Au nanocubes (Fig. 6.18, ~60 nm length) [57] and measured the DUV–FUV spectra of anatase TiO_2 with these Au nanocubes (Fig. 6.18). No significant differences between the spectrum of TiO_2 with Au nanocubes and that with the Au nanospheres of the corresponding size (60 nm diameter) were observed, indicating that the electronic-state changes are independent of the Au-nanoparticle shapes. We discuss reasons why the electronic states of TiO_2 with Au nanoparticles strongly depend on the Au size rather than on the Au shape.

As described in Sect. 6.3.1, upon the contact between TiO_2 and a metal, the electrons in TiO_2 are transferred to the metal. At the same time, a potential gradient is generated at the interface between TiO_2 and the metal, which prevents a recombination between the electrons in the metal and the holes in TiO_2, leading

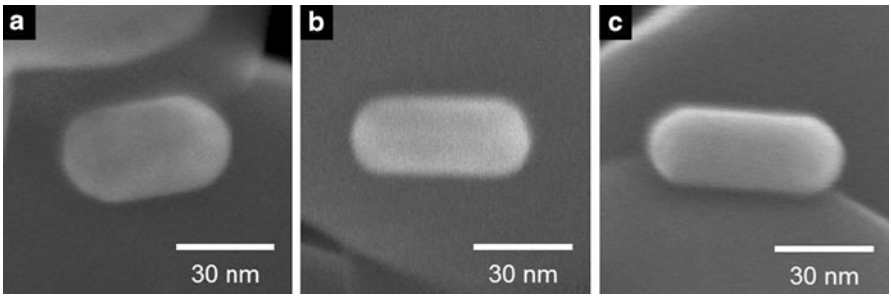

Fig. 6.16 SEM images of Au nanorods on TiO_2 with the following sizes: (**a**) 25 nm × 34 nm, (**b**) 25 nm × 47 nm, and (**c**) 25 nm × 60 nm

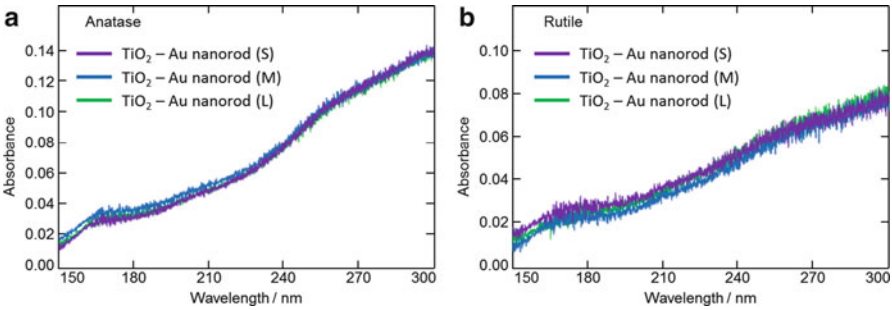

Fig. 6.17 DUV–FUV spectra of (**a**) anatase and (**b**) rutile TiO_2 modified with Au nanorods of various aspect ratios. The sizes of the Au nanorods are (S) 25 nm × 34 nm, (M) 25 nm × 47 nm, and (L) 25 nm × 60 nm

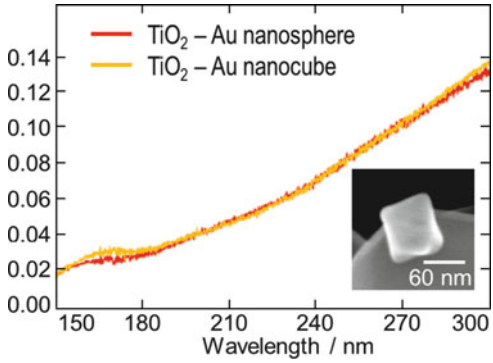

Fig. 6.18 DUV–FUV spectra of anatase TiO_2 modified with (*red*) Au nanospheres or (*yellow*) Au nanocubes. The SEM image of a deposited nanocube is also shown (*inset*)

to an enhancement of the charge-separation efficiency. The depth and width of the potential gradient depend on the Fermi levels, size, electric conductivity, and other properties of TiO_2 and the metal. In the present case, only the Au-nanoparticle size and shape were systematically changed. However, the width of the Au nanoparticle was not changed, i.e., the diameter of all the Au nanorods was maintained constant

at 25 nm. Therefore, the ATR spectra suggest that the width of the deposited Au nanoparticles may have a strong effect on the electronic states of TiO_2. Thus, we have discussed not only the effect of the size of Au nanoparticles in the wide range of 5–60 nm but also that of their shape.

6.6 Conclusions and Perspectives

By using our DUV–FUV spectroscopy method, we systematically studied the electronic states of TiO_2 alone and those of TiO_2 with metal nanoparticles.

The obtained naked TiO_2 spectra were in line with the previously reported reflection spectra and theoretical calculations (Sect. 6.2). The deposition of metal (Au, Pd, and Pt) nanoparticles significantly affected their spectral shape, indicating changes in the electronic states of TiO_2. A strong positive relationship was found between the degree of the spectral changes and the work function of the modified metal. Larger spectral changes indicate a stronger enhancement of charge separation, which in turn leads to an improvement of the photocatalytic activity of TiO_2 (Sect. 6.3). Anatase TiO_2 and rutile TiO_2 showed different spectra and spectral changes upon Pt-nanoparticle deposition. In particular, the photocatalytic activity of rutile TiO_2 showed a stronger enhancement than that of anatase TiO_2 (Sect. 6.4). Although a low shape dependence was observed, smaller Au nanoparticles induced larger electronic-state changes, leading to a higher photocatalytic activity (Sect. 6.5).

The results illustrated in this contribution clearly demonstrate the potential of DUV–FUV spectroscopy as a novel investigation method for the electronic states of various materials. Now, we are applying this method not only to TiO_2 but also to other materials (other semiconductors such as ZnO, organic phosphates, ion liquids, and so on). It is also important to confirm the electronic changes by other methods such as X-ray photoelectron spectroscopy (XPS) and ultraviolet photoelectron spectroscopy (UPS), which is in progress. The application of this method provides critical information about the enhancement mechanism and supports the development of high-efficiency optical materials such as photocatalysts and solar cells.

References

1. A.L. Linsebigler, G. Lu, J.T. Yates Jr., Chem. Rev. **95**, 735–758 (1995)
2. X. Chen, S.S. Mao, Chem. Rev. **107**, 2891–2959 (2007)
3. M.R. Hoffmann, S.T. Martin, W. Choi, D.W. Bahnemann, Chem. Rev. **95**, 69–96 (1995)
4. B. O'Regan, M. Grätzel, Nature **353**, 737–740 (1991)
5. M.K. Nazeeruddin, P. Péchy, T. Renouard, S.M. Zakeeruddin, R. Humphry-Baker, P. Comte, P. Liska, L. Cevey, E. Costa, V. Shklover, L. Spiccia, G.B. Deacon, C.A. Bignozzi, M. Grätzel, J. Am. Chem. Soc. **123**, 1613–1624 (2001)
6. P.V. Kamat, J. Phys. Chem. C **112**, 18737 (2008)

7. H. Tang, K. Prasad, R. Sanjinbs, P.E. Schmid, F. Lévy, J. Appl. Phys. **75**, 2042 (1994)
8. M.A. Fox, M.T. Dulay, Chem. Rev. **93**, 341–357 (1993)
9. M. Fujihira, Y. Satoh, T. Osa, Nature **293**, 206–208 (1981)
10. F. Gruy, M. Pijolat, J. Am. Ceram. Soc. **75**, 657–661 (1992)
11. A. Fujishima, X. Zhang, D.A. Tryk, Surf. Sci. Rep. **63**, 515–582 (2008)
12. A.-W. Xu, Y. Gao, H.-Q. Liu, J. Catal. **207**, 151–157 (2002)
13. W. Choi, A. Termin, M.R. Hoffmann, J. Phys. Chem. **98**, 13669–13679 (1994)
14. A. Hattori, K. Shimoda, H. Tada, S. Ito, Langmuir **15**, 5422–5425 (1999)
15. Z.H. Yuan, J.H. Jia, L.D. Zhang, Mater. Chem. Phys. **73**, 323–326 (2002)
16. B. Kraeutler, A.J. Bard, J. Am. Chem. Soc. **100**, 2239–2240 (1978)
17. T. Kawai, T. Sakata, Nature **282**, 283–284 (1979)
18. Y. Nosaka, K. Norimatsu, H. Miyama, Chem. Phys. Lett. **106**, 128–131 (1984)
19. U. Diebold, Surf. Sci. Rep. **48**, 53–229 (2003)
20. M. Jakob, H. Levanon, P.V. Kamat, Nano Lett. **3**, 353–358 (2003)
21. P.V. Kamat, J. Phys. Chem. Lett. **3**, 663–672 (2012)
22. G.E. Jellison Jr., L.A. Boatner, J.D. Budai, B.-S. Jeong, D.P. Norton, J. Appl. Phys. **93**, 9537–9541 (2003)
23. Y. Ozaki, Y. Morisawa, A. Ikehata, N. Higashi, Appl. Spectrosc. **66**, 1 (2012)
24. Y. Morisawa, T. Goto, N. Higashi, K. Takaba, N. Kariyama, A. Ikehata, Y. Ozaki, Rev. Sci. Instrum. **83**, 073103 (2012)
25. Y. Morisawa, T. Goto, A. Ikehata, N. Higashi, Y. Ozaki, *Encyclopedia of Analytical Chemistry* (Wiley, 2013), pp. 1–21
26. J. Zhang, M. Li, A. Feng, J. Chen, C. Li, J. Phys. Chem. B **110**, 927–935 (2006)
27. N. Higashi, A. Ikehata, Y. Ozaki, Rev. Sci. Instrum. **78**, 103107 (2007)
28. A. Ikehata, M. Mitsuoka, Y. Morisawa, N. Kariyama, N. Higashi, Y. Ozaki, J. Phys. Chem. A **114**, 8319–8322 (2010)
29. T. Goto, A. Ikehata, Y. Morisawa, N. Higashi, Y. Ozaki, Phys. Chem. Chem. Phys. **14**, 8097–8104 (2012)
30. Y. Morisawa, A. Ikehata, N. Higashi, Y. Ozaki, Chem. Phys. Lett. **476**, 205–208 (2009)
31. Y. Morisawa, A. Ikehata, N. Higashi, Y. Ozaki, J. Phys. Chem. A **115**, 562–568 (2011)
32. S. Tachibana, Y. Morisawa, A. Ikehata, H. Sato, N. Higashi, Y. Ozaki, Appl. Spectrosc. **65**, 221–226 (2011)
33. I. Tanabe, Y. Ozaki, Chem. Commun. **50**, 2117 (2014)
34. N. Hosaka, T. Sekiya, M. Fujisawa, C. Satoko, S. Kurita, J. Electron Spectrosc. Relat. Phenom. **78**, 75–78 (1996)
35. N. Hosaka, T. Sekiya, C. Satoko, S. Kurita, J. Phys. Soc. Jpn. **66**, 877–880 (1997)
36. R. Asahi, Y. Taga, W. Mannstadt, A.J. Freeman, Phys. Rev. B **61**, 7459–7465 (2000)
37. S. Sério, M.E. Melo Jorge, M.L. Coutinho, S.V. Hoffman, P. Limão-Vieira, Y. Nunes, Chem. Phys. Lett. **508**, 71–75 (2011)
38. Y. Borodko, S.E. Habas, M. Koebel, P. Yang, H. Frei, G.A. Somoriai, J. Phys. Chem. B **110**, 23052 (2006)
39. S. Teratani, J. Nakamichi, K. Taya, T. Tanaka, Bull. Chem. Soc. Jpn. **55**, 1688–1690 (1982)
40. I. Tanabe, T. Ryoki, Y. Ozaki, Phys. Chem. Chem. Phys. **16**, 7749 (2014)
41. K. Tanaka, M.F.V. Capule, T. Hisanaga, Chem. Phys. Lett. **187**, 73 (1991)
42. M. Landmann, E. Rauls, W.G. Schmidt, J. Phys. Condens. Matter **24**, 195503 (2012)
43. N. Xu, Z. Shi, Y. Fan, J. Dong, J. Shi, M.Z.-C. Hu, Ind. Eng. Chem. Res. **38**, 373 (1999)
44. Q. Zhang, L. Gao, J. Guo, J. Eur. Ceram. Soc. **20**, 2153 (2000)
45. S. Ikeda, N. Sugiyama, S. Murakami, H. Kominami, Y. Kera, H. Noguchi, K. Uosaki, T. Torimoto, B. Ohtani, Phys. Chem. Chem. Phys. **5**, 778 (2003)
46. J.I.L. Chen, G. von Freymann, V. Kitaev, G.A. Ozin, J. Am. Chem. Soc. **129**, 1196 (2007)
47. Z. Zhang, Z. Wang, S.-W. Cao, C. Xue, J. Phys. Chem. C **117**, 25939 (2013)
48. J. Zhang, L. Li, T. Yan, G. Li, J. Phys. Chem. C **115**, 13820 (2011)

49. I. Tanabe, T. Ryoki, Y. Ozaki, The effects of Au nanoparticle size (5-60 nm) and shape (sphere, rod, cube) over electronic states and photocatalytic activities of TiO_2 studied by far- and deep-ultraviolet spectroscopy. RSC Adv. **5**, 13648–13652 (2015)
50. M. Murdoch, G.I.N. Waterhouse, M.A. Nadeem, J.B. Metson, M.A. Keane, R.F. Howe, J. Llorca, H. Idriss, Nat. Chem. **3**, 489 (2011)
51. Y. Tian, T. Tatsuma, Chem. Commun., 1810 (2004)
52. Y. Tian, T. Tatsuma, J. Am. Chem. Soc. **127**, 7632 (2005)
53. K. Yu, Y. Tian, T. Tatsuma, Phys. Chem. Chem. Phys. **8**, 5417 (2006)
54. E. Kowalska, R. Abe, B. Ohtani, Chem. Commun., 241 (2009)
55. V. Subramanian, E.E. Wolf, P.V. Kamat, J. Am. Chem. Soc. **126**, 4943 (2004)
56. K. Qian, B.C. Sweeny, A.C. Johnston-Peck, W. Niu, J.O. Graham, J.S. Duchene, J. Qiu, Y.-C. Wang, M.H. Engelhard, D. Su, E.A. Stach, W.D. Wei, J. Am. Chem. Soc. **136**, 9842 (2014)
57. J. Zhang, C. Xi, C. Feng, H. Xia, D. Wang, X. Tao, Langmuir **30**, 2480 (2014)